STOYAN NEDELTCHEV

IDENTIFICATION OF CONSTANT AND STABLE MAIN TRANSITION VELOCITY IN BUBBLE COLUMN REACTORS

Institute of Chemical Engineering, Polish Academy of Sciences, Bałtycka 5, 44-100 Gliwice, Poland

This work presents new results about the reliable identification of the main transition velocity $U_{trans-1}$ in different bubble columns (0.1 – 0.46 m in inner diameter) equipped with several perforated plate gas distributors. Two different gas-liquid systems (air-water and air-therminol LT) have been used. The most important finding in this work is that $U_{trans-1}$ (end of the homogeneous regime) occurs at 0.04 $m \cdot s^{-1}$ irrespective of the operating conditions studied. For the $U_{trans-1}$ identification, the following parameters have been used: Kolmogorov and reconstruction entropies, degree of randomness and information entropy.
Keywords: bubble columns, flow regime identification, main transition velocity, entropy analysis

W pracy przedstawiono nowe wyniki dotyczące wiarygodnej identyfikacji głównej prędkości przejścia $U_{trans-1}$ w różnych kolumnach barbotażowych (o średnicy wewnętrznej 0,1 - 0,46 m) wyposażonych w kilka dystrybutorów gazu typu płyta perforowana. Zastosowano dwa różne układy gaz-ciecz (powietrze-woda i powietrze-therminol LT). Najważniejszym odkryciem w tej pracy jest to, że $U_{trans-1}$ (koniec reżimu przepływu homogenicznego) występuje dla prędkości 0,04 $m \cdot s^{-1}$ niezależnie od badanych warunków pracy. Do identyfikacji $U_{trans-1}$ wykorzystano następujące parametry: entropię Kołmogorowa, entropię rekonstrukcyjną, stopień losowości oraz entropię informacji.
Słowa kluczowe: kolumny barbotażowe, identyfikacja reżimu przepływu, główna prędkość przejścia

1. INTRODUCTION

Bubble columns (BCs) are simple but very effective (in terms of mass and heat transfer) gas-liquid reactors. They are frequently used in the chemical, petrochemical, biochemical and mining industries. In BCs such reactions as oxidations, chlorinations, hydrogenations, etc. are performed. In the BC design, the most important step is the selection of an effective gas distributor (GD) type. It determines both the initial and mean bubble diameter as well as the flow structures in the bubble bed (BB).

The influences of operating conditions, reactor geometry and physico-chemical properties of each phase on the reactor performance are not yet fully understood. That is why, both the BC design and scale-up is considered a difficult task. Vial et al. [1]

argue that it is still difficult to quantify the GD impact on the regime transitions. The complicated liquid hydrodynamics have a strong influence on mixing, heat and mass transfer and thus on the BC performance. The latter is affected by the prevailing flow regime (FR) and the quality of the gas distribution. The effect of the GD layout and regime transitions on the liquid hydrodynamics should be studied more systematically by means of the new advanced techniques (especially tomographic scans).

The superficial gas velocity U_g is the most important parameter in the BC operation. When the U_g value is below 0.04 $m \cdot s^{-1}$ (in the case of perforated plate (PP) gas sparger) the homogeneous (bubbly flow) regime prevails [2-3]. This FR is generated by porous plates or PP with small and closely spaced orifices [4]. The stable homogeneous flow regime begins when all orifices of the PP sparger form bubbles. Uniform layers of equally-sized small and rigid spherical or oblate ellipsoidal bubbles are continuously formed at the GD plate. The bubbles rise almost vertically and they agitate the BB. The homogeneous (bubbly flow) regime is observed at low U_g values. According to Simonnet et al. [5] this hydrodynamic regime is observed when the gas is uniformly distributed and the U_g value does not exceed 0.03 – 0.04 $m \cdot s^{-1}$. This conclusion will also be supported by the results in this work.

The homogeneous FR is characterized by a gentle agitation of the gas-liquid dispersion by means of relatively small uniform (spherical or ellipsoidal) bubbles, which rise vertically. The rise velocity of the bubbles in this FR is between 0.18 and 0.30 $m \cdot s^{-1}$ [2], depending on the mean bubble diameter and physico-chemical properties of the liquid. The bubble size distribution (BSD) is very narrow (essentially monomodal) and it is only affected by the GD layout. In other words, the BB hydrodynamics are strongly affected by the GD design. Bubble coalescence is insignificant. A relatively uniform and flat radial gas holdup profile and a rather flat liquid velocity profile are observed. The liquid moves upwards in the vicinity of the bubbles and downwards between the bubbles. No liquid macrostructure is observed [5]. In this FR there is inexistence of large-scale liquid circulations and only small liquid vortices are observed [6]. Flotation columns are normally operated at low U_g values, which maintain homogeneous (bubbly flow) conditions. As the U_g value increases, loss of the bubbly flow conditions is observed and this causes adverse effects on the BC performance. Thus, it is very important to identify the upper boundary of the homogeneous regime (so-called first transition velocity $U_{trans-1}$).

When the U_g value exceeds 0.03 – 0.04 $m \cdot s^{-1}$, the homogeneous FR becomes unstable and the transition regime is formed. This FR occurs because the transformation from the homogeneous to the heterogeneous FR is a gradual process. During the transition from bubbly flow to churn-turbulent flow, the bubble size increases rapidly due to bubble coalescence. The range of the transition regime depends on the column dimension, GD design and gas-liquid properties [7]. This FR is characterized by the formation of large macrostructures (large eddies) and widened BSD. In addition, both the gas holdup and liquid velocity profiles become parabolic. The transition regime corresponds to the development of local liquid circulation patterns in the column. The

occurrence and the persistence of the transition regime depends largely on both the uniformity and the quality of aeration. Simonnet et al. [5] argue that the transition regime is characterized by the existence of a central bubble stream, where bubbles move in an oscillating spiral manner and where large bubbles concentrate.

As the U_g value increases, the homogeneity is gradually deteriorated and ultimately destroyed by turbulence due to liquid circulations. The transition from the homogeneous to the heterogeneous FR is not a sudden event [4]. It is characterized with an intermittent character. The transition proceeds slowly and it is characterized by an increasing number of coherent structures (circulations, vortices, etc.) of increasing size and intensity within the BB. Chen et al. [8] argue that a vortical-spiral flow structure is formed in the transition regime and it disappears at higher gas flow rates (heterogeneous FR).

The homogeneous and heterogeneous FRs may coexist in the BB. The main transition velocity $U_{trans-1}$ has been identified by analyzing pressure signals, liquid velocity signals and by applying the drift-flux concept [4]. Several models for explanation of the onset of the transition regime have been proposed based on the bubble drag force [9], gas phase slip velocity [10], energy balance of the gas-liquid mixture [11] or the concept of small and large bubbles [12]. The predictive value of these models is rather poor [4]. A criterion for prediction of the main transition (end of homogeneous regime) has been developed by Shnip et al. [13] and Ruzicka et al. [4].

When the U_g value becomes higher than about 0.05 – 0.06 $m \cdot s^{-1}$, the flow structure in the transition regime reorganizes itself and the heterogeneous (churn-turbulent flow) regime is established. In this FR, there is a stronger turbulent motion of the gas bubbles and both bubble coalescence and break-up occur [7]. Larger spherical-cap (mushroom-like) bubbles and bubble clusters begin to form in the core and their wakes cause gross circulation patterns in the BB. The large bubbles are associated with the generation of eddies in the column. The onset of the heterogeneous FR is also associated with the formation of "coalescence-induced structures". Mudde et al. [14] reported the existence of coherent (or large-scale) structures (eddies, circulation cells, etc.).

The mass transfer in the heterogeneous FR is considerably different than the one in the homogeneous FR. The heterogeneous FR is characterized by a wide BSD, at least two bubble classes, vigorous mixing and the existence of a radial parabolic profile of both gas holdup and liquid velocity, which causes gross liquid circulation. The liquid phase develops highly chaotic and dynamic macro-scale circulation patterns [6]. In fact, in this FR a liquid macro-circulation exists, where the liquid ascends in the column center and descends near the column walls. This flow pattern (structure) is called "gulf steam" or "cooling tower" [6]. Several circulation cells [15] are also observed. In this FR, the GD layout plays a negligible role. Very often a spiral liquid flow pattern is observed. The liquid flow structure is much more chaotic and dynamic than in the previous two FRs. Industrial BCs mainly operate in the heterogeneous FR [7]. Therefore, the onset of this FR should be accurately identified.

The heterogeneous (churn-turbulent flow) regime is produced by either PP with small and closely spaced orifices at high U_g values or PP with large orifices at any U_g value [4]. In the first case, an instability of the homogeneous FR occurs at certain U_g value and this leads to the formation of the transition regime. The second case results from the non-uniform gas distribution at the PP due to the large orifices and their large spacing [4]. In the heterogeneous FR populations of large and highly non-uniform bubbles prone to coalesce are generated. The liquid flow pattern in the heterogeneous FR is substantially different than the one in the homogenous FR. Large-scale and strong non-uniformities in the BSD generate strong liquid convective motions within the entire BB – so-called gross liquid circulations [4]. High-voidage regions are accelerated and advected to the top where bubbles escape at the bed surface and the bubble-free liquid flows downwards near the walls.

The liquid circulations in the heterogeneous FR are highly non-stationary on short time scales [8,16]. The long-time radial profiles of liquid velocity and voidage are roughly parabolic as a function of column radius with a maximum on the centerline [17].

The available correlations [7,18,19] for prediction of the end of the homogeneous regime or the first transition velocity $U_{trans-1}$ do not take into account the effects of the GD layout, column diameter or the liquid height. In principle, the effects of the gas-liquid properties and the aspect ratio on the $U_{trans-1}$ values have not been studied exhaustively. However, Besagni and Inzoli [20] have included the three main BC design criteria into the most famous empirical correlations [18,19]. It is noteworthy that these authors identified the first transition velocities $U_{trans-1}$ based on simple methods, which are not very precise.

The aim of this work is to present new results, which reveal that the main transition velocity $U_{trans-1}$ is constant (it occurs at 0.04 $m \cdot s^{-1}$) and stable irrespective of the operating conditions tested. For this purpose, the nonlinear chaos analysis will be used for calculating both the Kolmogorov entropy (KE) and degree of randomness (DR).

2. IDENTIFICATION METHODS

2.1. KOLMOGOROV ENTROPY

The Kolmogorov entropy (KE) is the most important parameter in the nonlinear chaos analysis. This chaotic invariant can provide important insights into the complex hydrodynamics of BCs. Nonlinear chaos analysis can be used for a quantitative characterization of various regime transitions in a BC.

The BC can be regarded as a chaotic system [21], that is, as a system governed by nonlinear interactions between the system variables. Due to the nonlinearity, this deterministic system is sensitive to small changes in initial conditions and is, therefore, characterized by a limited predictability. The dynamics of the chaotic system are fully

represented by the so-called strange attractor („imaginary figure") in the phase space. The attractor of the chaotic system (so-called „chaotic attractor") is not finite and the system never returns to the same state. Van den Bleek and Schouten [22] developed a reliable technique for attractor reconstruction. A typical feature of the nonlinear system is that it spontaneously develops time-dependent behavior. The chaotic system differs considerably from the system usually encountered, especially with respect to its predictability. It has been shown that BCs [21] and fluidized beds [22] are chaotic systems.

The KE quantifies the degree of unpredictability of the system. The KE value reflects the rate of information loss of the system, and thus accounts for the accuracy of the initial conditions that is required to predict the evolution of the system over a given time interval [22]. KE > 0 is a sufficient condition for chaos, and to some extent the chaotic system is only predictable over a restricted time interval. KE is large for very irregular dynamic behavior, small in the case of more regular, periodic-like behavior, and zero for completely periodic systems. This parameter is sensitive to changes in operating conditions and as such, can be employed for FR identification. The study of BCs as chaotic systems has provided new conceptual and theoretical tools enabling a better understanding of their complex behavior. For a nonlinear system such as a BC, a small change in a key parameter can lead to sudden and dramatic changes in both the qualitative and quantitative behavior of the system. For one value, the behavior might be periodic, whereas for another value only slightly different from the first, the behavior might be completely aperiodic (it never exactly repeats). Some sudden and dramatic changes in the nonlinear system may give rise to the complex behavior called chaos. The time-dependent (or transient) behavior of the BC is described as chaotic when that behavior is aperiodic and is apparently random. Hence, the focus of this paper is to demonstrate that the nonlinear chaos analysis (the KE concept) can be applied successfully to tomographic (Computed Tomography (CT) and Nuclear Gauge Densitometry (NGD)) data obtained in a BC for the sake of identification of the boundaries of various FRs. To the best of the author's knowledge, the nonlinear chaos analysis is applied for the first time to nonintrusive CT data. By means of the chaos theory, attempts to extract information hidden in the CT and NGD signals will be presented. The transition velocities determined by means of the KE values will be compared with those identified by means of the information entropy (IE) theory.

Schouten et al. [23] have developed an algorithm for maximum-likelihood estimation of KE. According to it, KE is a function of the sampling frequency f_s and the mean b value, which is the average number of steps needed for the exponential divergence of two imaginary (state) vectors:

$$KE = -f_s \ln (1-b_{mean}^{-1}) \tag{1}$$

Random vectors are generated and the distance between each vector pair is calculated and compared with a preselected parameter called cut-off length L. The latter is set proportional to the average absolute deviation (AAD), which is a standard statistical parameter. It is a robust statistical estimator of the data width around the mean. For

instance, one can start generating state vectors from the first element x_1 with embedding dimension 50 and time delay of unity. The following vectors can be generated: ($x_1 \ldots x_{50}$), ($x_{51} \ldots x_{100}$), ($x_{101} \ldots x_{150}$), ($x_{151} \ldots x_{200}$), etc. Then the first vector pairs could be set with an element difference of 100-vector ($x_1 \ldots x_{50}$) will be compared with vector ($x_{101} \ldots x_{150}$), then vector ($x_{51} \ldots x_{100}$) with vector ($x_{151} \ldots x_{200}$) and so on. Another random vector generation could be based on element difference of 200, 300, 400, etc. The time series has consisted of 10 000 points. The distance between the vector pairs has been estimated on the basis of the maximum norm definition [23]. This means that the absolute differences between the corresponding elements in each vector are calculated and then the maximum value is considered as the distance between the two vectors. It is compared with the cut-off length and it is less than L, then we increase with one element the two vectors and compare again the distance between them. The number of such steps before the vector distance becomes higher than L gives one b value. At least 10 000 b_{mean} values are needed for reliable KE calculation (with error less than 1 %). The definition of the state vectors, their dependence on the embedding dimension and the delay time are explained in [23].

2.2. DEGREE OF RANDOMNESS

This new parameter has been defined by Nedeltchev et al. [24]. It is based on the nonlinear chaos theory. Again the signal is reconstructed into different vectors and multiple vector pairs are generated. The difference between the elements of the vectors is fixed at 100. No other vector combination is considered. All the vector pairs with a distance higher than the preselected cut-off length L are counted. The ratio of this number of vector pairs to the total number of generated vector pairs yields the degree of randomness (DR). This parameter is dimensionless and it varies from 0 to 1. This index is selected since it shows a well-pronounced local minimum at every transition velocity. The spatial DR is just a modification of the DR algorithm and it is defined in [24]. The x-ray scans from the ultrafast x-ray tomography are divided into multiple semi-rings and the time series in each entity are analyzed based on the generation of state vector pairs with a distance of 100 between their elements. If only in one entity the vector pair distance is lower than L and in the others this is not the case, then b is equal to 1. If we have two such cases, then b is equal to 2 and so on. The total number of b cases equal to 1 divided by the sum of these b=1 values plus the other b values (higher than 1) yields the spatial DR. It also varies between 0 and 1. The algorithm is very well explained with an example (in table form) in Nedeltchev et al. [24].

2.3. INFORMATION ENTROPY

The information entropy (IE) algorithm is explained exhaustively in Nedeltchev and Shaikh [25]. It is based on the estimation of the probability, information amount and their product. In this work, the IE algorithm was applied to the vector pairs gener-

ated from the reconstructions based on chaos analysis. In the case of 10000 photon counts measured by Computed Tomography (CT), 99 vector pairs were generated with a difference between the elements set equal to 100. The probability P was calculated as a ratio of the number N_v of vector pairs with a distance smaller than L to total number of generated vector pairs.

$$P = N_V / N \tag{2}$$

The information amount IA is a negative logarithmic function of the probability:

$$IA = - \log (P) \tag{3}$$

The IE (type 1) is a product of both P and IA. The IE (type 2) has been defined on the basis of the reconstruction of the signal into two different parts consisting of 5000 elements and comparison of the absolute difference between each two elements from the two parts. The cases with an absolute difference less than L were divided by 5000 (total number of element pairs) in order to obtain the probability. Then the rest of the IE algorithm was applied.

2.4. RECONSTRUCTION ENTROPY

The reconstruction entropy (RE) algorithm has been explained by Nedeltchev [26]. Basically, the signal has been divided into two equal parts and the absolute difference between the elements (from both parts) has been calculated. It is noteworthy that the elements are not organized into vectors in this approach. It has been compared with the cut-off length L (set proportional to the AAD) and the number of element pairs with a distance smaller than L have been taken into account. When there are repeating cases with an absolute difference less than L this forms one b value (the number of steps before the absolute difference becomes higher than L). When all b values are estimated, then b_{mean} is calculated and Eq. (1) is used to extract the RE value. This means that an exponential divergence of the element pairs has been assumed.

3. EXPERIMENTAL SETUPS

3.1. DIFFERENTIAL PRESSURE (DP) FLUCTUATIONS

The differential pressure (DP) fluctuations were measured in a BC (0.1 m in ID) operated with nitrogen-tap water system at ambient conditions (temperature=293 K and pressure=0.1 MPa). The column was equipped with a perforated plate (PP) gas sparger (19 orifices, d_0 = 1.0 mm, OA = 1.0 %). One leg of the DP transducer (Labom GmbH, Germany) was installed at an axial position z of 0.65 m. The other leg was connected to the top of the column. The sampling frequency was set at 100 Hz. Fig. 1

shows an example (first 500 points (5 s)) of DP fluctuations at U_g =0.027 m·s^{-1}. The schematic of the facility is shown in [25].

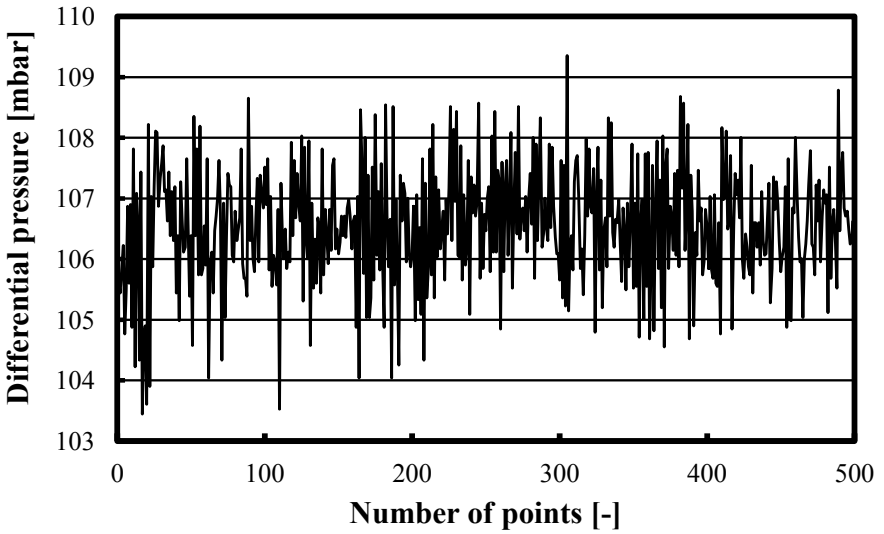

Fig. 1. DP fluctuations in a BC (0.1 m in ID) operated with a nitrogen-tap water system at U_g=0.027 m·s^{-1}.

3.2. GAUGE PRESSURE (GP) FLUCTUATIONS

The gauge pressure (GP) fluctuations were measured by means of GP transducer PX409 (Omega Eng., USA) installed at z = 1.05 m in a BC (0.14 m in ID) operated with an air-deionized water system at ambient conditions (temperature=293 K and pressure=0.1 MPa). The BC was equipped with a PP gas sparger (121 orifices, d_0 = 1.32 mm, OA = 1.08 %). The f_s value was fixed at 67 Hz.

3.3. COMPUTED TOMOGRAPHY (CT)

The Computed tomography (CT) facility consists of a radioactive source (Cs-134) and five scintillation detectors. In the middle of the BC (0.162 m in ID) the radioactive source was placed at one side of the column and five scintillation detectors (made of NaI) were mounted at the opposite side. The CT facility was capable of rotating at 360^0 and multiple scans of the gas-liquid dispersion from all possible angles were performed. More information is provided in Nedeltchev et al. [27].

The gamma-ray photon counts (shown in [26]) from the central scintillation detector were treated by both the IE and RE algorithms. The sampling frequency was set at

20 Hz. The BC was equipped with a PP gas sparger (163 orifices × Ø 1.32 mm, OA=1.09 %). The column operated with an air-therminol LT system at ambient conditions (temperature=293 K and pressure=0.1 MPa).

3.4. NUCLEAR GAUGE DENSITOMETRY (NGD)

The same CT facility was used. However, only one scintillation detector was centrally positioned against the radioactive source (Cs-134). The NGD facility was static, i.e. the source and the detector were not rotating around the column. After the opening of the radioactive source, the gamma rays penetrated through the gas-liquid dispersion and were recorded by the scintillation detector (made of NaI). The sampling frequency was set at 50 Hz. More information (including photon count time series) is provided in Nedeltchev et al. [28]. A smaller air-distilled water BC (0.1 m in ID) was used. The column was equipped with a PP gas sparger (64 orifices × Ø 1.32 mm, OA=1.09 %). Only scans at ambient conditions (temperature=293 K and pressure=0.1 MPa) were performed.

3.5. X-RAY TOMOGRAPHY

X-ray tomographic facility was used to record the X-ray passings through a small air-distilled water BC (0.1 m in ID, clear liquid height H_0 =0.66 m) operated at ambient conditions. X-rays passing the BC were recorded by a very fast multi-pixel X-ray arc detector co-aligned with the target. The x-ray tomographic facility can provide useful information (including the bubble size and its distribution) about the multiphase flow. The x-ray scans (shown in [29]) were performed at an axial height of 0.5 m with a sampling frequency of 1000 Hz (ultrafast operation). At each U_g value 29 000 subsequent images were recorded. More information about the facility's operating principle is provided in Nedeltchev et al. [29]. Only x-ray scans at ambient conditions (temperature=293 K and pressure=0.1 MPa) were performed.

4. RESULTS AND DISCUSSION

Fig. 2 shows that the KE profile (extracted from DP fluctuations at z = 0.65 m) in a narrow nitrogen-tap water BC (0.1 m in ID) is capable of identifying two transition velocities U_{trans} in the U_g range between 0.014 and 0.041 $m \cdot s^{-1}$. The BC was equipped with a PP gas distributor (19 orifices, d_0 = 1.0 mm). Two well-pronounced local KE minima are observed at U_g = 0.023 and 0.039 $m \cdot s^{-1}$. The first one distinguishes the boundary between the gas maldistribution regime and the homogeneous FR. The second minimum identifies the onset of the transition FR. It is noteworthy that these critical U_{trans} values are strictly valid for the preselected key parameters (cut-off length = 3AAD, delay time of unity and embedding dimension = 50) for extraction of the KE

values. Fig. 2 shows that there are some conditions, which are characterized with the same KE values (degree of chaos), so they should correspond to the same hydrodynamics. For instance, at U_g = 0.018 and 0.021 m·s^{-1} the KE values are practically the same as the ones at U_g = 0.027, 0.029 and 0.031 m·s^{-1}.

Fig. 3 shows that the DR profile is also capable of identifying the two U_{trans} values (based on two local minima), however, they occur at somewhat different U_g values. According to the DR values, the gas maldistribution regime ends at U_g = 0.027 m·s^{-1}. In comparison to the KE result, this is a deviation of 17.4 %. Fig. 3 shows that the onset of the transition FR occurs at U_g = 0.039 m·s^{-1}, which result coincides with the one in Fig.2. It is noteworthy that the DR values at U_g = 0.027, 0.033, 0.035 and 0.037 m·s^{-1} are practically the same.

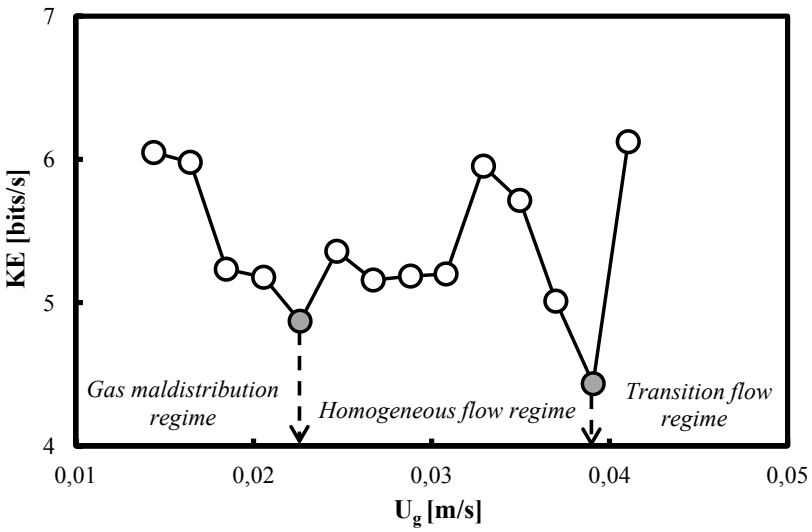

Fig. 2. KE profile as a function of U_g in a small nitrogen-tap water BC (0.1 m in ID) equipped with a PP gas sparger (19 orifices × Ø 1 mm).

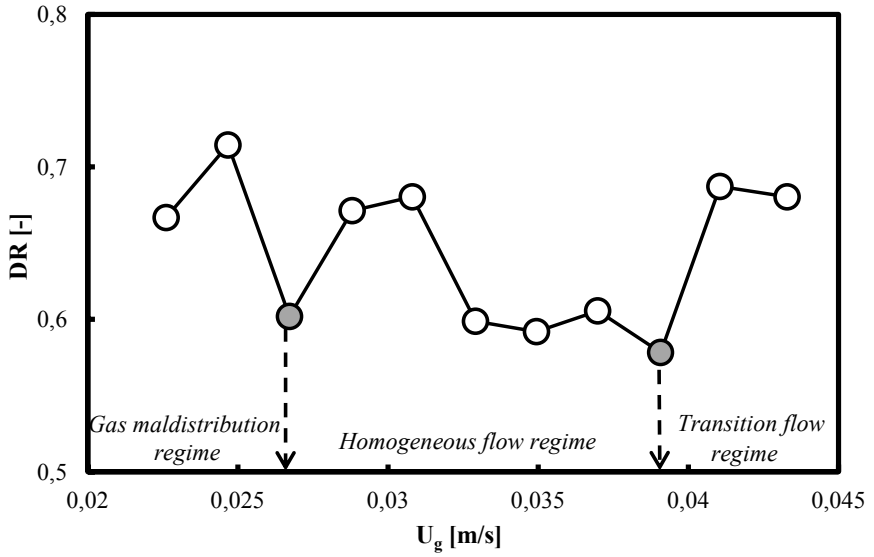

Fig. 3. DR profile as a function of U_g in a small nitrogen-tap water BC (0.1 m in ID) equipped with a PP gas sparger (19 orifices × Ø 1 mm).

Fig. 4a shows that the IE (type 1) extracted from photon counts (recorded by a centrally positioned detector against the gamma-ray source) measured by CT in a BC (0.162 m in ID) operated with an air-therminol LT system can also identify successfully the boundary between homogeneous FR and transition FR. The BC has been equipped with a PP gas sparger (163 orifices, d_0 = 1.32 mm). At U_g = 0.04 m·s^{-1} a well-pronounced local IE (type 1) minimum is observed. Before this critical velocity the IE (type 1) values monotonously decrease, while above it the IE (type 1) values constantly increase. Fig. 4b shows that in the case of profiles of IE (type 2) and RE, the first transition velocity $U_{trans-1}$ is also identifiable at U_g = 0.04 m·s^{-1}. Both parameters exhibit a well-pronounced local minimum at this critical gas velocity. Fig. 4b clearly demonstrates that below $U_{trans-1}$ the IE (type 2) values monotonously decrease and this IE (type 2) behavior characterizes the homogeneous FR. Beyond 0.04 m·s^{-1} the IE (type 2) values steadily increase and this is an indication for the formation of a new hydrodynamic regime, i.e. the transition FR.

A comparison between the results in Figs. 2-3 and Figs. 4a-b reveal that the type of gas-liquid system, the column diameter and the orifice diameter do not have a significant effect on the boundary between the homogeneous FR and transition FR. This result has been confirmed by analyzing x-ray scans in a small air-distilled water BC (0.1 m in ID) equipped with a PP gas sparger (55 orifices, d_0 = 0.5 mm). Fig. 5 shows that in this gas-liquid system the onset of the transition FR occurs at U_g = 0.04 m·s^{-1}.

So, even when an orifice diameter of 0.5 mm is used, the main transition velocity is not changed.

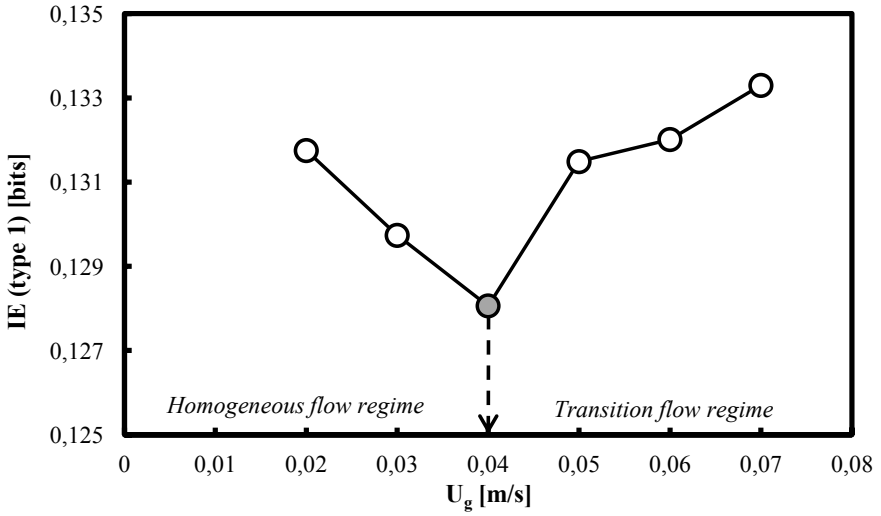

Fig. 4a. IE (type 1) profile as a function of U_g in an air-therminol LT BC (D_C=0.162 m in ID, H_0 =2.0 m) equipped with a PP gas sparger (163 orifices × Ø 1.32 mm).

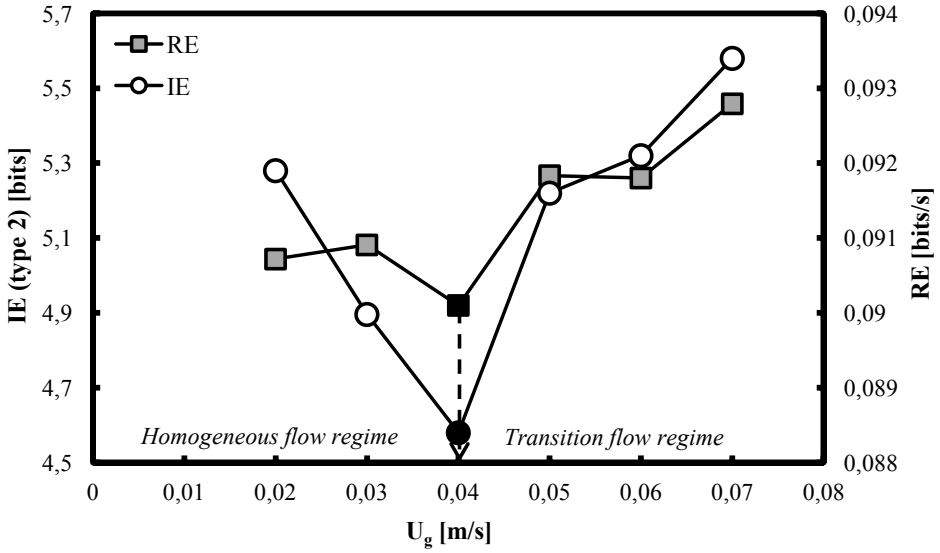

Fig. 4b. Profiles of IE (type 2) and RE as a function of U_g based on CT data in a BC (D_C = 0.162 m, H_0 = 2.0 m) operated with an air-therminol LT system.

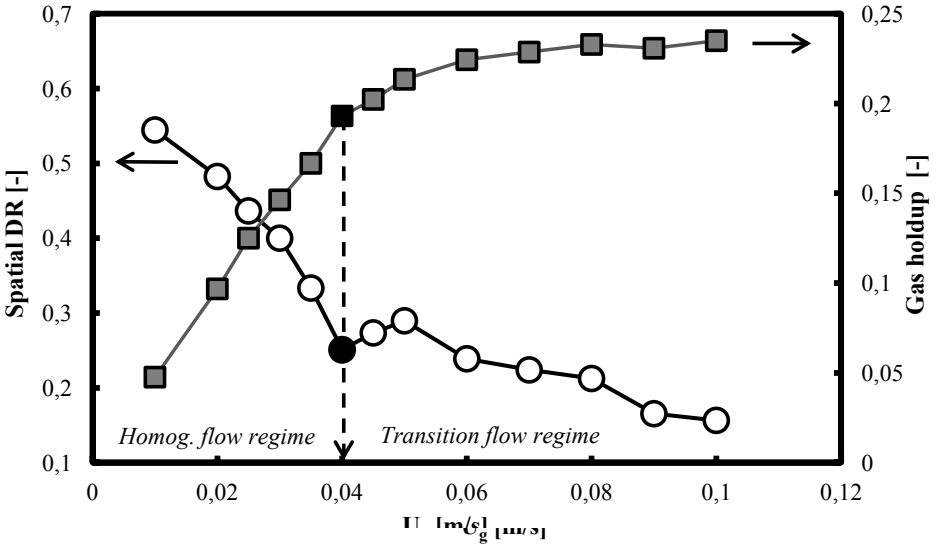

Fig. 5. Spatial DR profile as a function of U_g in an air-distilled water BC (0.1 m in ID) equipped with a PP gas sparger (55 orifices × Ø 0.5 mm, H_0 = 0.66 m).

In order to support the above-mentioned findings, the previous similar results (in cylindrical BCs) reported in the literature will be summarized. Hyndmann et al. [30] have reported a $U_{trans-1}$ value of 0.038 m·s^{-1} in an air-water BC (0.2 m in ID, H_0 = 1.4 m) equipped with a PP gas sparger: 69 orifices, d_0 = 1.0 mm, OA = 0.17 %. Zahradnik and Fialová [31] reported that in an air-water BC (0.14 m in ID) the first transition velocity $U_{trans-1}$ occurs at U_g = 0.04 m·s^{-1}. The BC was equipped with a PP gas sparger (157 orifices, d_0 = 0.5 mm, OA = 0.2 %). Vial et al. [1] reported that when a small BC (0.1 m in ID) equipped with a multiple-orifice gas sparger (50 orifices, d_0 = 1 mm) is used, then the homogeneous flow conditions prevail up to U_g = 0.04 m·s^{-1}.

The KE profile extracted from NGD data [28] in a narrow BC (0.1 m in ID) confirms that the onset of the transition FR occurs at U_g = 0.04 m·s^{-1}. The column has been equipped with a PP gas sparger (64 orifices, d_0 = Ø 1.32 mm, OA = 1.09 %). Fig. 6 exhibits a well-pronounced local KE minimum at this critical gas velocity. It is noteworthy that in the imperfect homogeneous FR the KE values monotonously increase. This KE behavior was modelled by Nedeltchev et al. [28].

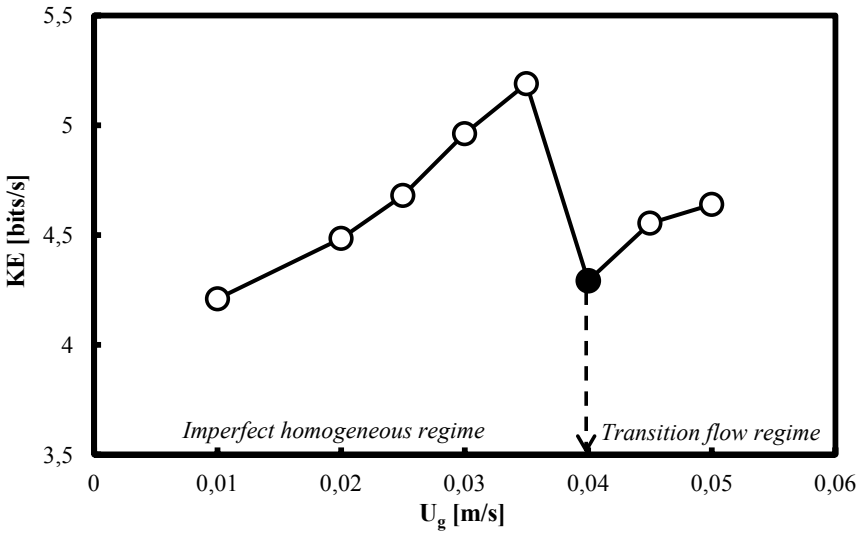

Fig. 6. KE profile (from NGD data) as a function of U_g in an air-distilled water BC (0.1 m in ID) equipped with a PP gas sparger (64 × Ø 1.32 mm, H_0 = 1.2 m, OA = 1.09 %).

The KE values extracted from GP fluctuations in an air-deionized water BC (0.14 m in ID) confirm the finding that the first transition velocity $U_{trans-1}$ occurs at U_g = 0.04 m·s^{-1}. The column has been equipped with a PP gas sparger (121 orifices, d_0 = 1.32 mm, OA = 1.08 %). The onset of the transition FR is distinguishable based on the well-pronounced local KE minimum (see Fig. 7).

The KE profile extracted from GP fluctuations recorded at z = 1.05 m (clear liquid height: 1.91 m) in a large BC (0.46 m in ID) equipped with a PP gas sparger (241 orifices, d_0 = 3.0 mm, OA = 1.09 %) reveals that the end of the homogeneous FR occurs at U_g = 0.039 m·s^{-1}. Fig. 8 shows that a well-pronounced local KE minimum occurs at this critical gas velocity ($U_{trans-1}$). In addition, the DR profile (see Fig. 8) exhibits also a local minimum at U_g = 0.039 m·s^{-1}. This critical gas velocity $U_{trans-1}$ is in agreement with the result (0.04 m·s^{-1}) of Zahradnik and Fialová [31].

In table 1 are summarized the obtained results. Columns with four different diameters have been used. Four different gas-liquid systems have been investigated. PP gas spargers with six different number of orifices and four different orifice diameters d_0 have been tested. All these conditions corresponded to a first transition velocity $U_{trans-1}$ in the range of 0.039-0.04 m·s^{-1}. The next step in the near future would be to find a suitable dimensionless number, which remains constant for all these operating conditions.

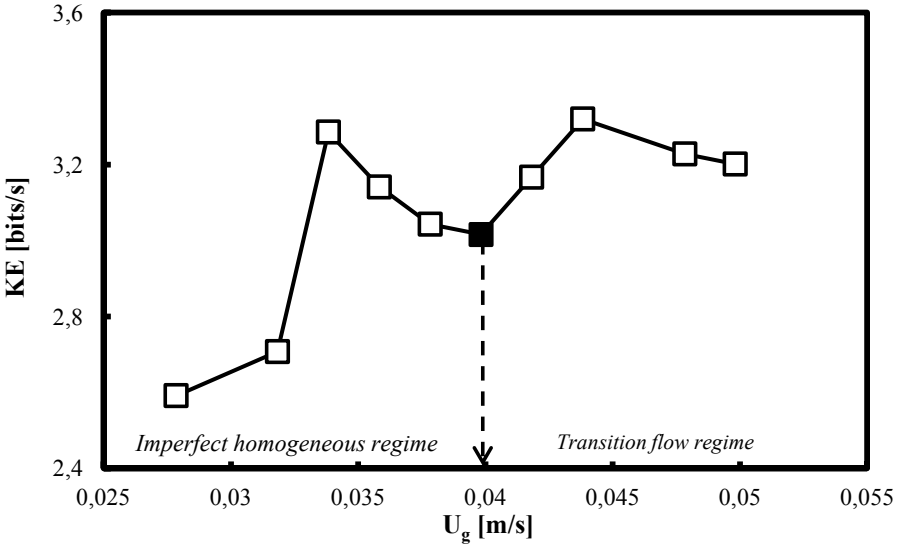

Fig. 7. KE profile (from GP fluctuations) as a function of U_g in an air-deionized water BC (0.14 m in ID) equipped with a PP gas sparger (121 × Ø 1.32 mm, OA = 1.08 %).

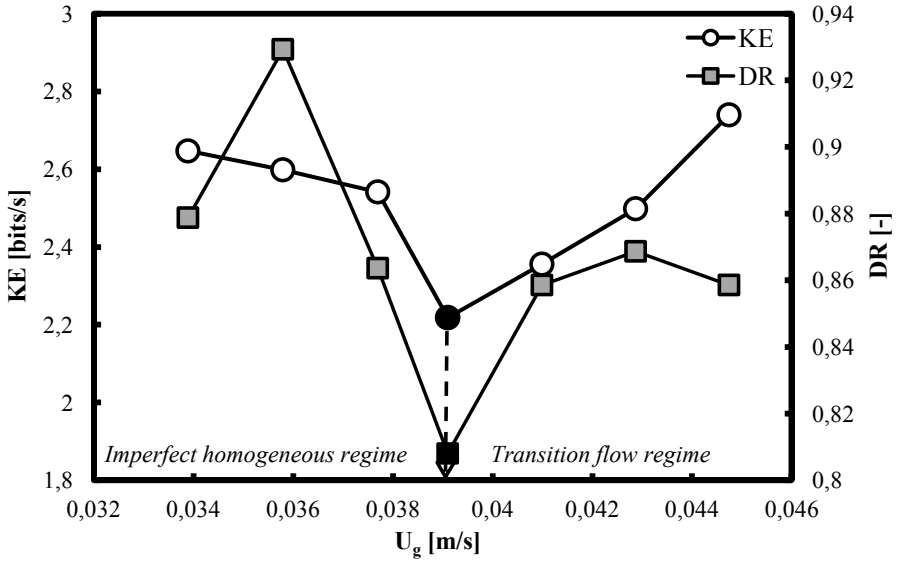

Fig. 8. KE profile (from GP fluctuations) as a function of U_g in an air-deionized water BC (0.46 m in ID) equipped with a PP gas sparger (241 orifices × Ø 3.0 mm, OA = 1.09 %).

Table 1. Summary of the operating conditions and constant $U_{trans-1}$ value

D_c, m	d_0, mm	Number of orifices	$U_{trans-1}$, m/s	Gas-liquid system
0.1	1.0	19	0.039	Nitrogen-tap water
0.162	1.32	163	0.040	Air-therminol LT
0.1	0.5	55	0.040	Air-distilled water
0.1	1.32	64	0.040	Air-distilled water
0.14	1.32	121	0.040	Air-deionized water
0.46	3.0	241	0.039	Air-deionized water

CONCLUSIONS

The first transition velocity $U_{trans-1}$ in BCs has been identified by means of new and advanced methods. Based on various measurements with different experimental techniques, the following conclusions have been drawn:

- The first transition velocity $U_{trans-1}$ occurs at 0.04 $m \cdot s^{-1}$ irrespective of the column diameter and gas distributor layout (orifice diameter and number of orifices);
- The reported results in the article imply that the $U_{trans-1}$ value is independent of or a weak function of the physicochemical properties of the liquid;
- The article provides information about the most powerful identification method for every signal used;

SYMBOLS

b – number of steps before two vectors (or two element pairs) deviate, -
b_{mean} – mean b value from the reconstructions, -
d_0 – orifice diameter, m
D_c – column diameter, m
DR – degree of randomness, -
H_0 – clear liquid height, m
IA – information amount, -
IE – information entropy, bits
KE – Kolmogorov entropy, bits s^{-1}
L – cut-off length, -
N_V – number of vector pairs with a distance smaller than L, -

N – total number of vector pairs generated, -
P – probability, -
U_g – superficial gas velocity, m s^{-1}
U_{trans} – transition velocities, m s^{-1}
$U_{trans-1}$ – main transition velocity, m s^{-1}
z – axial position, m

ABBREVIATIONS

AAD – average absolute deviation
BB – bubble bed
BC – bubble column
BSD – bubble size distribution
CT – computed tomography
DP – differential pressure
FR – flow regime
GD – gas distributor
GP – gauge pressure
NGD – nuclear gauge densitometry
OA – open area
PP – perforated plate

REFERENCES

[1] Vial, Ch., Lainé, R., Poncin, S., Midoux, N., Wild, G., 2001. Influence of gas distribution and regime transitions on liquid velocity and turbulence in a 3-D bubble column. Chem. Eng. Sci., 56, 1085-1093.
[2] Shah, Y. T., Kelkar, B. G., Godbole, S. P., Deckwer, W.-D., 1978. Design Parameters Estimations for Bubble Column Reactors. AIChE J., 28, 353-379.
[3] Leonard, C., Ferrasse, J.-H., Boutin, O., Lefevre, S., Viand, A., 2005. Bubble column reactors for high pressures and high temperatures operation. Chem. Eng. Res. Des., 100, 391-421. http://dx.doi.org/10.1016/j.cherd.2015.05.013.
[4] Ruzicka, M. C., Zahradnik, J., Drahoš, J., Thomas, N. H., 2001. Homogeneous-heterogeneous regime transition in bubble columns. Chem. Eng. Sci., 56, 4609-4626.
[5] Simmonet, M., Gentric, C., Olmos, E., Midoux, N., 2008. CFD simulation of the flow field in a bubble column reactor: importance of the drag force formulation to describe regime transitions. Chem. Eng. & Process., 47, 1726-1737.
[6] Diaz, M. E., Montes, F. J., Galán, M. A., 2008. Experimental study of the transition between unsteady flow regimes in a partially aerated two-dimensional bubble column. Chem. Eng. & Process., 47, 1867-1876.
[7] Im, H., Park, J., Lee, J. W., 2019. Prediction of main regime transition with variations of gas and liquid phases in a bubble column. ACS Omega, 4, 1329-1343.
[8] Chen, R. C., Reese, J., Fan, L.-S., 1994. Flow structure in a three-dimensional bubble column and three-phase fluidized bed. AIChE J., 40, 1093-1104.
[9] Riquarts, H. P., 1979. Model representation of homogeneous and heterogeneous two-phase flow in fluidized beds and bubble columns. Germ. Chem. Eng., 2, 268-274.
[10] Joshi, J. B., Lali, A. M., 1984. Velocity-hold up relationship in multiphase contactors-a unified approach. Frontier in Chem. Reac. Eng., 1, 314-329.
[11] Gharat, S. D., Joshi, J. B., 1992. Transport phenomena in bubble column reactors II. Chem. Eng. J., 48, 153-166.

[12] Krishna, R., Wilkinson, P. M., Van Dierendonck, L. L., 1991. A model for gas holdup in bubble columns incorporating the influence of gas density on flow regime transitions. Chem. Eng. Sci., 46, 2491-2496.

[13] Shnip, A. I., Kolhatkar, R. V., Swamy, D., Joshi, J. B., 1992. Criteria for the transition from the homogeneous to the heterogeneous regime in two-dimensional bubble column reactors. Int. J. Multiphase Flow, 17, 18, 705-726.

[14] Mudde, R. F., Lee, D. J., Reese, J., Fan, L.-S., 1997. Role of coherent structures on Reynolds stresses in a 2-D bubble column. AIChE J., 43, 913-926.

[15] Joshi, J. B., Axial mixing in multiphase contactors: a unified correlation. Trans. Inst. Chem. Eng., 58, 155-165.

[16] Devanathan, N., Dudukovic, M. P., Lapin, A., Lubbert, A., 1995. Chaotic flow in bubble column reactors. Chem. Eng. Sci., 50, 2661-2667.

[17] Franz, K., Borner, T., Kantorek, H. J., Buchholz, R., 1984. Flow structures in bubble columns. Germ. Chem. Eng., 7, 365-374.

[18] Wilkinson, P. M., Spek, A. P., Van Dierendonck, L. L., 1992. Design parameters estimation for scale up of high pressure bubble columns. AIChE J., 38, 544-554.

[19] Reilly, I. G., Scott, D. S., De Bruijn, T. J. W., MacIntyre, D., 1994. The role of gas phase momentum in determining gas holdup and hydrodynamic flow regimes in bubble column operations. Can. J. Chem. Eng., 72, 3-12.

[20] Besagni, G., Inzoli, F., 2017. Novel gas holdup and regime transition correlation for two-phase bubble columns. J. Phys.: Conf. Ser., 923, 012011.

[21] Letzel, H. M., Schouten, J. C., Krishna, R., Van den Bleek, C. M., 1997. Characterization of regimes and regime transitions in bubble columns by chaos analysis of pressure fluctuations. Chem. Eng. Sci., 52, 4447-4459.

[22] Van den Bleek, C. M., Schouten, J. C., 1993. Deterministic chaos: a new tool in fluidized bed design and operation. Chem. Eng. J., 53, 75-87.

[23] Schouten, J. C., Takens, F., Van den Bleek, C. M., 1994. Maximum-likelihood estimation of the entropy of an attractor, Phys. Rev. E Stat. Phys Plasmas Fluids Relat. Interdisc. Top., 49, 126-129.

[24] Nedeltchev, S., Top, Y., Hlawitschka, M., Schubert, M., Bart, H.-J., 2020. Identification of the regime boundaries in bubble columns based on the degree of randomness in the signals. Can. J. Chem. Eng., 98, 1607-1621. DOI: 10.1002/cjce.23719.

[25] Nedeltchev, S., Shaikh, A., 2013. A new method for identification of the main transition velocities in multiphase reactors based on information entropy theory. Chem. Eng. Sci., 100, 2-14. http://dx.doi.org/10.1016/j.ces.2013.03.039.

[26] Nedeltchev, S., 2015. New methods for flow regime identification in bubble columns and fluidized beds. Chem. Eng. Sci., 137, 436-446. http://dx.doi.org/10.1016/j.ces.2015.06.054.

[27] Nedeltchev, S., Shaikh, A., Al-Dahhan, M., 2006. Flow regime identification in a bubble column based on both statistical and chaotic parameters applied to computed tomography data. Chem. Eng. & Techn. 29, 1054-1060. DOI: 10.1002/ceat.200600162.

[28] Nedeltchev, S., Shaikh, A., Al-Dahhan, M., 2011. Flow regime identification in a bubble column via nuclear gauge densitometry and chaos analysis. Chem. Eng. Technol., 34, 225-233. 10.1002/ceat.201000308.

[29] Nedeltchev, S., Schubert, M., Hampel, U., 2017. Extraction of information and reconstruction entropies from ultrafast X-ray tomography data in a bubble column. Chem. Eng. Sci., 170, 225-233. http://dx.doi.org/10.1016/j.ces.2017.03.020.

[30] Hyndman, C. L., Larachi, F., Guy, C., 1997. Understanding gas-phase hydrodynamics in bubble columns: a convective model based on kinetic theory. Chem. Eng. Sci., 52, 63-77.

[31] Zahradnik, J., Fialova, M., 1996. The effect of bubbling regime on gas and liquid phase mixing in bubble column reactors. Chem. Eng. Sci., 51, 2491-2500.

STOYAN NEDELTCHEV

OKREŚLENIE STAŁEJ I STABILNEJ PRĘDKOŚCI PRZEJŚCIOWEJ W REAKTORACH BARBOTAŻOWYCH

Stopień wymieszania oraz transport ciepła i masy w kolumnach barbotażowych (BC) zależą od granic głównych reżimów przepływu. W pracy przedstawiono nowe, najbardziej wiarygodne metody identyfikacji głównej prędkości przejścia pomiędzy reżimami $U_{trans-1}$ w kilku BC, wyposażonych wyłącznie w dystrybutory gazu typu płyta perforowana. Badaniom poddano BC dla czterech różnych średnic kolumny i średnic otworów, a także sześciu różnych liczb otworów. Kolumny pracowały w warunkach otoczenia. Wykazano, że wartości entropii Kołmogorowa (KE) można wiarygodnie wyodrębnić z 10 000 zliczeń fotonów (zarejestrowanych za pomocą nieinwazyjnej densytometrii jądrowej (NGD)), a następnie wykorzystać do oznaczenia $U_{trans-1}$. Na podstawie dobrze zaznaczonego lokalnego minimum w profilu KE w BC (średnica kolumny D_c = 0,1 m) pracującej w układzie powietrze - woda dejonizowana stwierdzono, że $U_{trans-1}$ występuje dla prędkości 0,04 $m \cdot s^{-1}$. Wybrano najbardziej odpowiednie parametry dla dokładnych obliczeń KE (długość odcięcia, wymiar osadzania i opóźnienie czasowe). Profil KE został również wyodrębniony z wahań ciśnienia różnicowego (DP) zarejestrowanych w kolumnie o małej skali (Dc = 0,1 m), pracującej w układzie azot - woda wodociągowa. W porównaniu z ustawieniami dla uzyskania KE z danych NGD, tylko długość odcięcia (proporcjonalna do średniego odchylenia bezwzględnego) była nieco inna. Stwierdzono, że granica reżimu homogenicznego pojawia się dla 0,039 $m \cdot s^{-1}$. Poniżej prędkości gazu na pełny aparat U_g = 0,023 $m \cdot s^{-1}$ stwierdzono nieprawidłową dystrybucję gazu. Te dwie prędkości przejścia zostały potwierdzone przez nowy parametr zwany stopniem losowości (DR). Granica wyznaczająca koniec reżimu jednorodnego przepływu przy 0,039 $m \cdot s^{-1}$ została potwierdzona, natomiast koniec zakresu nieprawidłowej dystrybucji gazu nastąpił nieco później, przy 0,027 $m \cdot s^{-1}$.

Profil KE został również wyodrębniony z wahań ciśnienia zarejestrowanych w kolumnie dużej skali (D_c = 0,46 m), pracującej w układzie powietrze - woda dejonizowana w warunkach otoczenia. W porównaniu z poprzednimi przypadkami (wyniki NGD i DP), jedynie długość odcięcia była nieco inna. Ponownie wystąpiło dobrze zaznaczone lokalne minimum przy 0,04 $m \cdot s^{-1}$, wyznaczające granicę reżimu homogenicznego.

W przypadku kolumny o średnicy D_c = 0,162 m pracującej w układzie powietrze-therminol LT, dwa typy entropii informacji (IE) i entropii rekonstrukcyjnej potwierdziły, że granica $U_{trans-1}$ wystąpiła dla 0,04 $m \cdot s^{-1}$. Te trzy parametry uzyskano z 10 000 zliczeń fotonów zarejestrowanych przez centralny detektor (umieszczony naprzeciw źródła promieniotwórczego) z nieinwazyjnej tomografii komputerowej (CT).

Na końcu opracowano nowy parametr zwany przestrzennym stopniem losowości (*spatial degree of randomness*, SDR) w celu wyodrębnienia wartości $U_{trans-1}$ z nieinwazyjnych ultraszybkich tomogramów rentgenowskich. Wyniki SDR dla małej kolumny (D_c=0,1 m, powietrze - woda destylowana) potwierdziły, że główna prędkość przejścia występuje przy 0,04 $m \cdot s^{-1}$ niezależnie od zarówno średnicy kolumny i otworu, jak i układu gaz-ciecz. To główny wniosek z bieżącej pracy.

Porównanie z ustaleniami kilku innych grup badawczych potwierdza istotność i dokładność rezultatów, przedstawionych w niniejszym artykule.

Received: 16.11.2020